NANO LETTERS

pubs.acs.org/NanoLett

Letter

Dynamically Tunable All-Weather Daytime Cellulose Aerogel Radiative Supercooler for Energy-Saving Building

Chenyang Cai,[⊥] Zechang Wei,[⊥] Chunxiang Ding, Bianjing Sun, Wenbo Chen, Christoph Gerhard, Evgeny Nimerovsky, Yu Fu,* and Kai Zhang*

Cite This: *Nano Lett.* 2022, 22, 4106−4114

Read Online

ACCESS | Metrics & More | Article Recommendations | Supporting Information

ABSTRACT: A passive cooling strategy without any electricity input has shown a significant impact on overall energy consumption globally. However, designing tunable daytime radiative cooler to meet requirement of different weather conditions is still a big challenge, especially in hot, humid regions. Here, a novel type of tunable, thermally insulating and compressible cellulose nanocrystal (CNC) aerogel coolers is prepared via chemical cross-linking and unidirectional freeze casting process. Such aerogel coolers can achieve a subambient temperature drop of 9.2 °C under direct sunlight and promisingly reached the reduction of ∼7.4 °C even in hot, moist, and fickle extreme surroundings. The tunable cooling performance can be realized via controlling the compression ratio of shape-malleable aerogel coolers. Furthermore, energy consumption modeling of using such aerogel coolers in buildings in China shows 35.4% reduction of cooling energy. This work can pave the way toward designing high-performance, thermal-regulating materials for energy consumption savings.

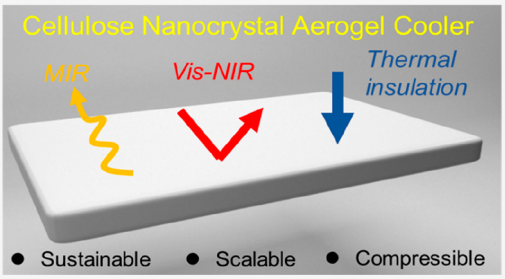

KEYWORDS: *aerogel cooler, daytime radiative cooling, all-weather, cellulose nanocrystal, tunable*

The development of efficient cooling technology based on environmentally friendly and biobased materials is one of the key points to relieve energy consumption and global warming. Air conditioners, as traditional cooling systems, usually consume large amounts of energy and emit lots of greenhouse gases.[1] In comparison, passive radiative-cooling materials dissipate heat through an atmospheric transparent window (8−13 μm) to the atmosphere without any energy consumption,[2−4] which can show great application in energy-savings buildings,[5] wearable cooling textiles,[6,7] and cooling systems on farms.[8] Although remarkable progress in enhanced infrared emissivity and improved cooling ability have been made, daytime radiative cooling (especially direct under sunlight) represents a great challenge because of the strong solar absorption over infrared emission, which results in parasitic heat transfer.

To solve this problem, daytime radiative cooling materials have been proposed, such as photonic structures,[9] hybrid metamaterials,[10] organic coatings,[11] microporous polymer films,[8,12] plastic textiles,[13] and white woods,[14] to reflect most of the sunlight such that the heat absorption from the sun is below the level of radiative cooling. To date, the subambient daytime cooling performance is still strongly limited compared to its theoretical potential because of the heating of diverse radiative coolers with the whole environment by the sun, especially in summer.[15−17] In addition, almost all the daytime radiative coolers showed good performance in arid surroundings and at relatively low environmental humidity. However, the atmospheric humidity and complex weather (cloud cover or wind speed) heavily influence the absorbed power density of atmospheric radiation and the magnitude of the cooling performance.[18] Therefore, it is still a big challenge to develop high-performance coolers for practical daytime thermal radiation applications in all weather conditions, especially for hot and humid regions.

To address these challenges, a type of thermal-insulating aerogel coolers based on cross-linked cellulose nanocrystals (CNCs) was designed and realized for the first time, which generates efficient cooling by fulfilling the requirements at the molecular level and nano-/microscale. Such efficient thermal-regulating aerogel coolers, simultaneously acting as a thermal insulator and a daytime passive radiative cooler, integrate dual functions in one design. The development of such CNC aerogel coolers is based on four key points: (1) strong solar reflectance throughout the solar spectrum (0.25−2.5 μm); (2) high and selective infrared emittance in the mid-infrared region (8−13 μm) because of the presence of C−O−C and C−O bonds in cellulose;[19,20] (3) construction of aerogels with ultralow thermal conductivity to reduce thermal convection from ambient

Received: March 1, 2022
Revised: April 28, 2022
Published: May 5, 2022

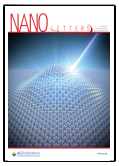

https://doi.org/10.1021/acs.nanolett.2c00844
Nano Lett. 2022, 22, 4106−4114

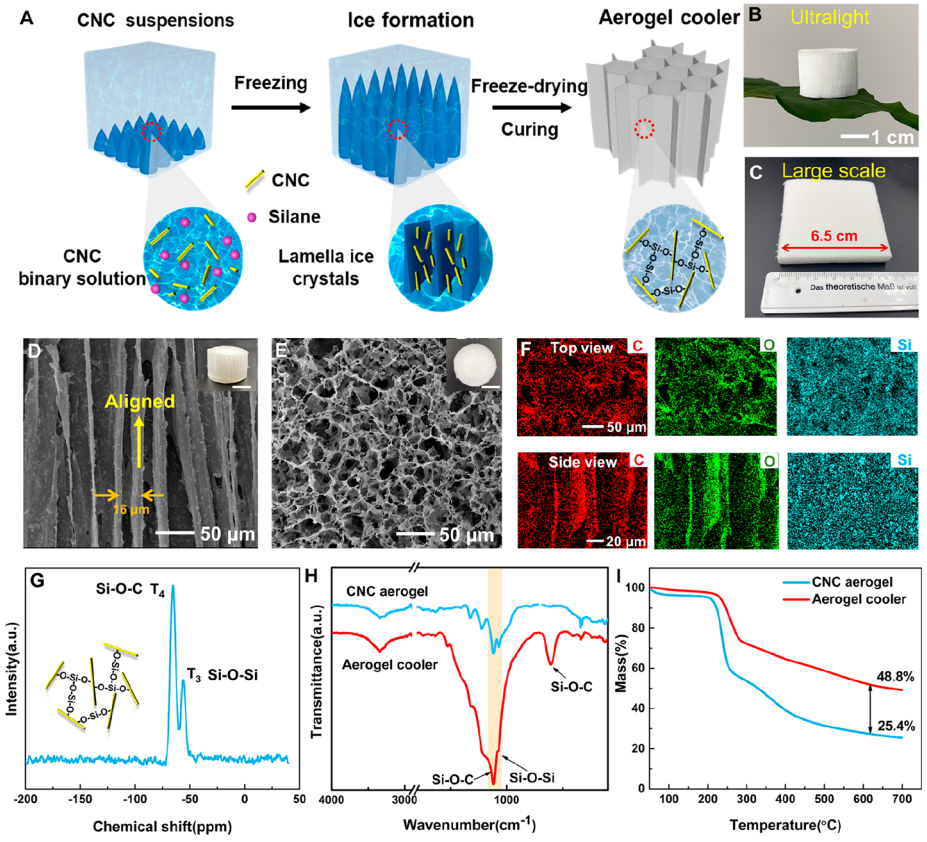

Figure 1. Construction and characterization of aerogel coolers. (A) Preparation process for aerogel coolers. (B) Ultralight nature. (C) Upscaling potential. (D) Interior structure of aerogel coolers. The scale bar of inset picture is 1 cm. (E) Top surface morphology of aerogel coolers. The scale bar of inset picture is 1 cm. (F) Mapping images of aerogel coolers in top view and side view. (G) ^{29}Si solid-state NMR spectrum of aerogel cooler. (H) FTIR curves of an aerogel from pristine CNCs and an aerogel cooler. (I) TGA curves of a CNC aerogel and an aerogel cooler.

surroundings to the inner space; and (4) mechanical robustness to meet the increasing demand for harsh conditions. The first two requirements are satisfied by using sustainable CNCs and a silane agent as building blocks. Taking advantage of a cross-linking reaction between CNCs and silane agent, a large number of chemical bonds including C−H, C−O, Si−O−Si, and C−O−C bonds are beneficial for highly radiative cooling performance. To satisfy the last two criteria, we combined the unique properties of a stiff−flexible cross-linked network with the unidirectional freeze-casting method to yield a three-dimensional network with aligned network structures.

As the building blocks of the aerogel coolers, CNCs were prepared via the hydrolysis process with H_2SO_4 and well-dispersed in water at the concentration of 5 mg/mL ascribing to surface-attached SO_3^--groups.[21] CNCs typically showed a rigid rod shape with an average length of 367 ± 43 nm and an average width of 14 ± 3 nm (Figure S1). Subsequently, a silane agent methyltrimethoxysilane (MTMS) added in CNC suspensions cross-linked CNCs by reacting with OH-groups on their surface (Figure 1A). Part of the MTMS simultaneously generated SiO_2 nanoparticles that were also homogenized in the sol (Figure S2), yielding the well-dispersed suspensions. Then, the dispersion was instantly frozen by using unidirectional freezing approach to prepare aerogel coolers. Different from pristine CNC aerogels with poor mechanical stability (Figure S3), a homogeneously cross-linked network of Si−O−Si and Si−O−C bonds was formed after the condensation of MTMS and CNCs. Interestingly, the porous hierarchical structure endowed the aerogel coolers with the ultralight character, yielding a density of around 9.4 mg/cm^3 (Figures 1B and S4). The aerogels can be molded into different shapes, such as solid cylinder, solid cube and cuboid (Figure S5). Moreover, facile upscaling of the fabrication is feasible (Figure 1C).

Scanning electron microscopy (SEM) was used to evaluate the surface and interior structure of the aerogel coolers. The aerogel coolers displayed an obvious porous topology as well as interconnected pores as observed from cross-section, which is similar to that in previous studies using freeze-casting (Figure 1D).[22,23] The aerogel coolers also exhibited unique aligned channels with anchored SiO_2 nanoparticles across the longitudinal section (Figure 1E). The porous and longitudinal aligned channels are formed due to the directional ice growth during the unidirectional freezing step. As shown in Figure 1F and Tables S3 and S4, the C, O, and Si elements were identically detected in mapping images (cross-sectional and longitudinal sections), which further indicates the cross-linked homogeneous CNC-silane networks. The cross-linking can be further verified by the obvious two peaks at −56 and −66 ppm in the solid-state ^{29}Si NMR spectrum, which are explained by 3D cross-linked siloxane network.[24] As well, the FT-IR spectrum of the cross-linked network in aerogel cooler shows increased relative intensity of the bands at 1033 and 1105 cm^{-1} (Figure 1H), which can be explained by the formation of Si−O−C and Si−O−Si chemical bonds.[25] Compared with pristine CNC aerogels, the aerogel coolers exhibited excellent thermal stability by showing a higher initial decomposition temperature (215 °C) and carbon residue (48.8%), respectively (Figure 1I).

https://doi.org/10.1021/acs.nanolett.2c00844
Nano Lett. 2022, 22, 4106−4114

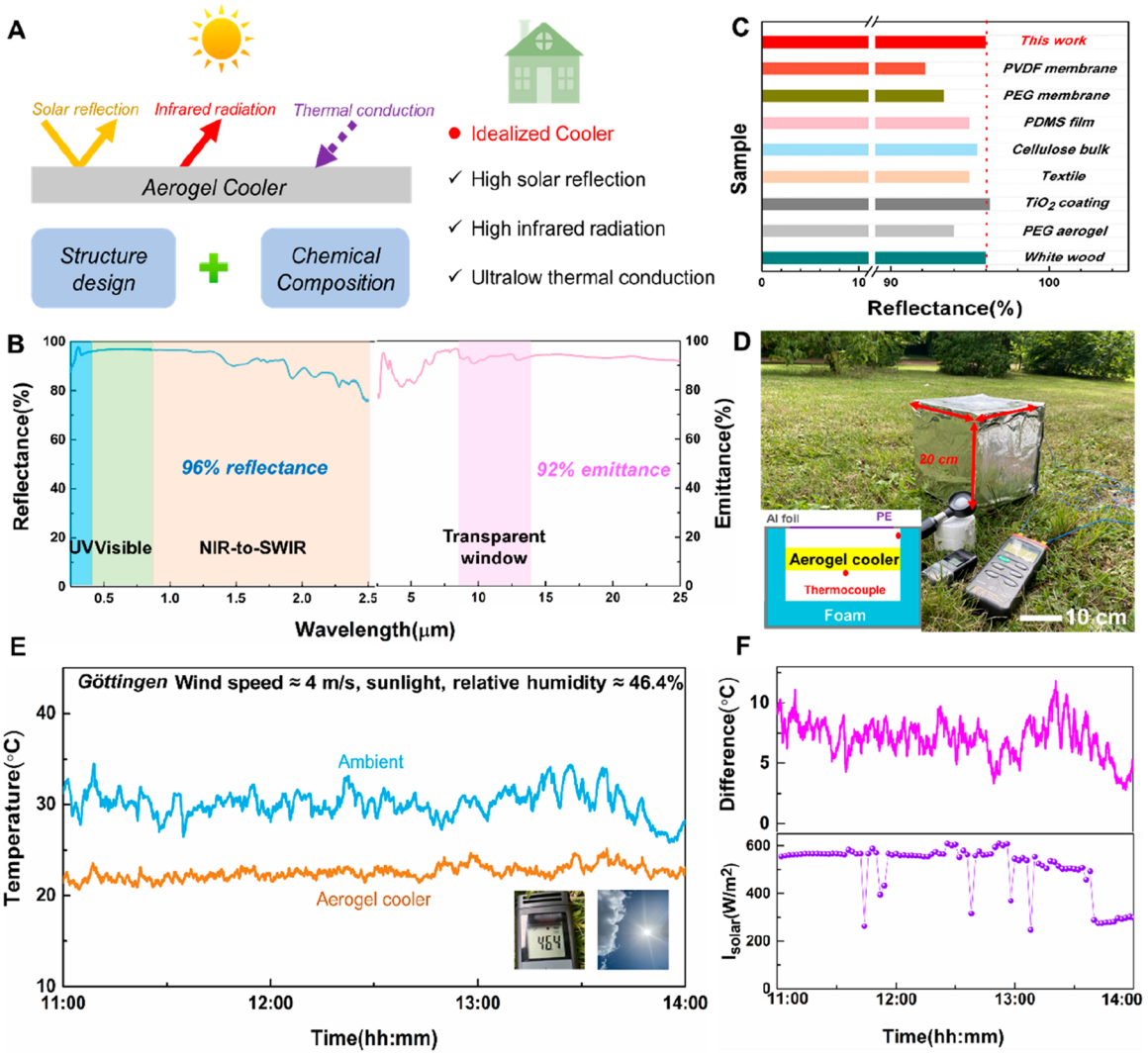

Figure 2. Daytime radiative cooling performance of aerogel coolers. (A) Proposed mechanism of outstanding cooling performance of aerogel coolers. (B) Spectral UV−visible−infrared reflectance/emittance of aerogel coolers presented against the AM1.5 solar spectra and the atmospheric transparent window. (C) Comparison of solar reflectance with other cooling materials. (D) Optical image of self-made thermal box. (E) Real-time temperature data of the outdoor experiment with an aerogel cooler in Göttingen (11 June 2021, 51°33′31.1″ N, 9°57′26.1″ E). (F) Corresponding subambient temperature drop (ΔT) and solar intensity.

Different from traditional coolers, our thermal-insulating CNC aerogel coolers integrate high solar reflectivity, high emissivity, and low thermal conduction in one design, which synergistically contribute to dramatic decrease of the parasitic heat transfer (Figure 2A). In particular, the white color of CNC aerogels indicated the superior scattering property of visible light, which can be explained by the chemical structure of CNCs (Figure 1C,E). Thanks to the chemical bonding and morphology design strategy, the aerogel coolers showed a high reflectivity of 96% in the visible-light region (0.3−2.5 μm) and high emissivity of 92% during the atmospheric transparent window (8−13 μm), as measured in real-time measurements (Figure 2B), which is much higher than that of most other radiative cooling materials in previous studies (Figure 2C).[3,13,14,16,26−29] The strong infrared emission in the 8−13 μm region is mainly attributed to the complex infrared emission of chemical bonds of C−H, C−O, C−O−C, Si−O−Si, and Si−O−C stretching vibrations in the aerogel cooler.

The real radiative cooling property of aerogel coolers (12 mm) was characterized in Göttingen (51°33′32″ N, 9°57′27″ E) in June with a clear sky by using a custom-made thermal box in the environment with a wind speed of ∼4 m/s and a relative humidity of ∼46.4%. As shown in Figure 2D, a custom-made thermal box has been designed to test the cooling performance according to previous work.[3,26] The ambient temperature, solar power intensity, relative humidity, and aerogel cooler temperature were all recorded in real time (Figures 2E and S7). In the daytime, the aerogel coolers showed a subambient temperature drop of $|\Delta T| \approx 9.2$ °C even under the peak solar intensity of near 600 W/m^2 at noon from 11:00 a.m. to 2:00 p.m. (Figure 2E,F). Also during the night, the aerogel coolers exhibited good cooling performance, resulting in cooling to ∼5.3 °C below ambient temperature (Figure S8). We also evaluated the cooling performance of aerogel coolers on different surfaces, as shown in Figure S9. The cooling performance of the top surface of the aerogel cooler is slightly better than that of the bottom and side surface.

The principal mechanism of infrared radiation based on designed chemical-bonds in our system was shown in Figure 3A. The chemical bonds of C−O−C (1100 cm^{-1}) and C−C (900

https://doi.org/10.1021/acs.nanolett.2c00844
Nano Lett. 2022, 22, 4106−4114

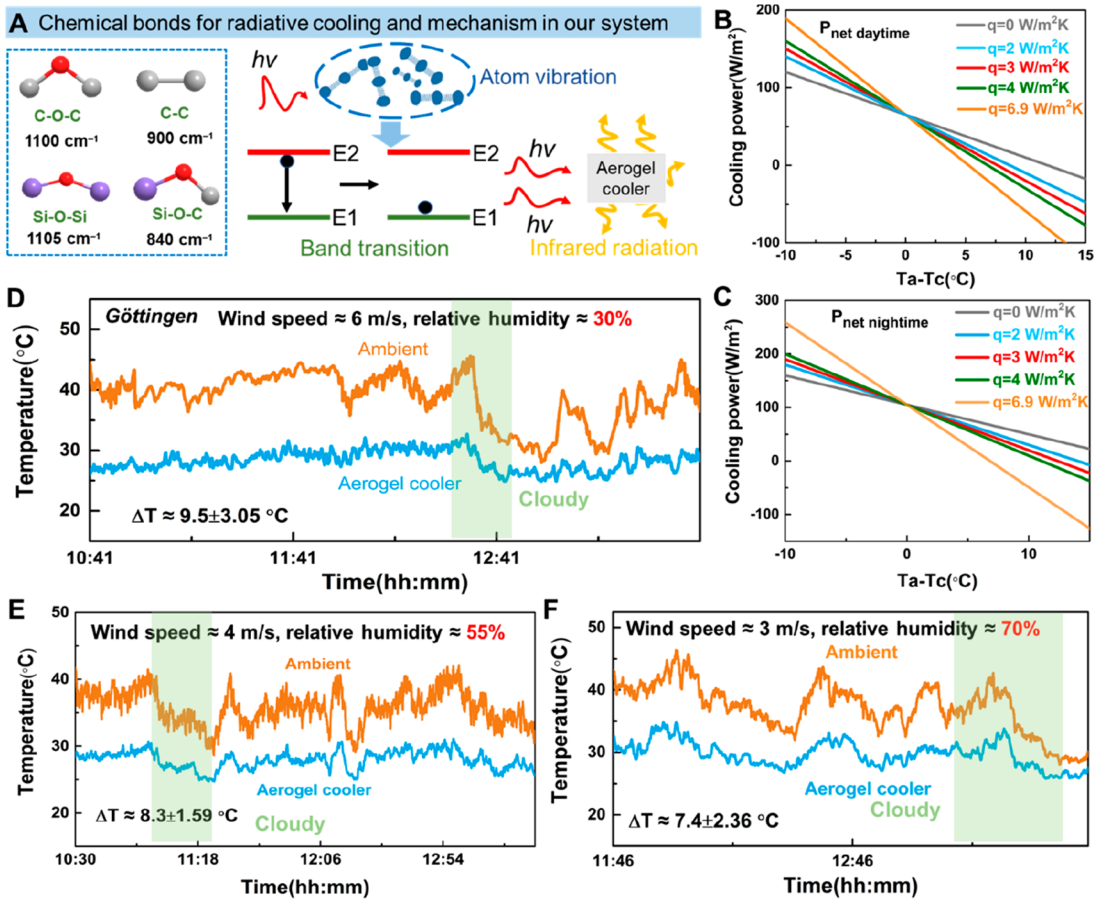

Figure 3. Proposed mechanism and all-weather radiative cooling performance. (A) Chemical bonds and proposed mechanism of radiative emittance of aerogel cooler. (B) Calculated cooling power of aerogel cooler (daytime). (C) Calculated cooling power of aerogel cooler (nighttime). (D) Cooling performance of aerogel coolers at a wind speed of 6 m/s and a relative humidity of 30%. (E) Cooling performance of aerogel coolers at a wind speed of 4 m/s and a relative humidity of 55%. (F) Cooling performance of aerogel coolers at a wind speed of 3 m/s and a relative humidity of 70%.

cm^{-1}) of CNC skeleton, as well as new positive chemical bonds of Si−O−C (840 cm^{-1}) and Si−O−Si (1105 cm^{-1}) generated from the cross-linking reaction between CNC and silane agent show strong stretching vibration in mid-infrared region. Upon the as-prepared aerogel cooler receiving the external radiation energy ($h\nu$) from its outside surroundings, it can accelerate molecular motion, and the inner atoms will undergo strong stretching vibration. Meanwhile, the electrons at the high-energy band will transition to the low-energy band, which can result in releasing photons. Finally, the aerogel cooler can emit heat in the form of electromagnetic waves in the mid-infrared region.

The net daytime (P_{net_day}) and nighttime (P_{net_night}) cooling powers (P_{net}) of a radiative cooler can be calculated based on the following equations,[30−32] respectively (detailed calculation methods are shown in the Supporting Information). As noted, the P_{net} at $T_a - T_c = 0$ is the net cooling power of aerogel cooler at ambient temperature ($P_{net}(T_a = T_c)$), which is not affected by the q. Meanwhile, the $T_a - T_c$ at $P_{net} = 0$ is the maximum cooling temperature reached ($(T_a - T_c)$max). As shown in Figure 3B,C, the P_{net} of the aerogel cooler during the daytime is lower than that of nighttime. This can be explained by that the solar heating process can exist during the daytime because the R_{solar} is still 4% less than 100%. Specifically, the $(T_a - T_c)$ max of the aerogel cooler can reach up to ∼11.5 °C during the daytime under direct sunlight without nonradiative heat. A $(T_a - T_c)$ value of ∼14 °C of the aerogel cooler can be also achieved during the heat of the night ($q = 0$). More importantly, a big temperature drop of ∼6 °C can be still achieved during the daytime even with a nonradiative heat coefficient of 6.9 W m^{-2} K^{-1}.

The real-world radiative cooling performance is affected by different weather parameters, such as relative humidity, wind speed, and cloud cover. Benefiting from surface roughness and low surface energy of silane cross-linked CNC aerogel, aerogel coolers showed an enhanced hydrophobicity (water contact angle of around 138° in Figure S10). On the basis of dynamic mechanical analysis at different relative humidity, the storage modulus shows a relatively durable trend with 70% retention at 80% relative humidity compared to that at 20% relative humidity, highlighting its excellent humidity-adaptive property (Figure S10). This stability of aerogel coolers allows their application under diverse climate conditions, especially at high relative humidity.

We choose three days with different wind velocities (3, 4, and 6 m/s), relative humidity (from 30% to 55% to 70%, Figures S11−S13, Supporting Information Note S1) and cloud cover to conduct experiments. With a wind speed of 6 m/s and 30% relative humidity, the average subambient cooling of ∼9.5 ± 3.05 °C was observed (Figure 3D). With a wind speed of 4 m/s and a relative humidity of 55%, an average subambient cooling of ∼8.3 ± 1.59 °C was observed (Figure 3E). It is noteworthy that a temperature decrease of ∼7.4 ± 2.36 °C was realized under a high relative humidity of 70% and dramatically changed weather conditions (sunny−cloudy−sunny−cloudy) (Figure 3F). Such excellent performance of the aerogel coolers under various

https://doi.org/10.1021/acs.nanolett.2c00844
Nano Lett. 2022, 22, 4106−4114

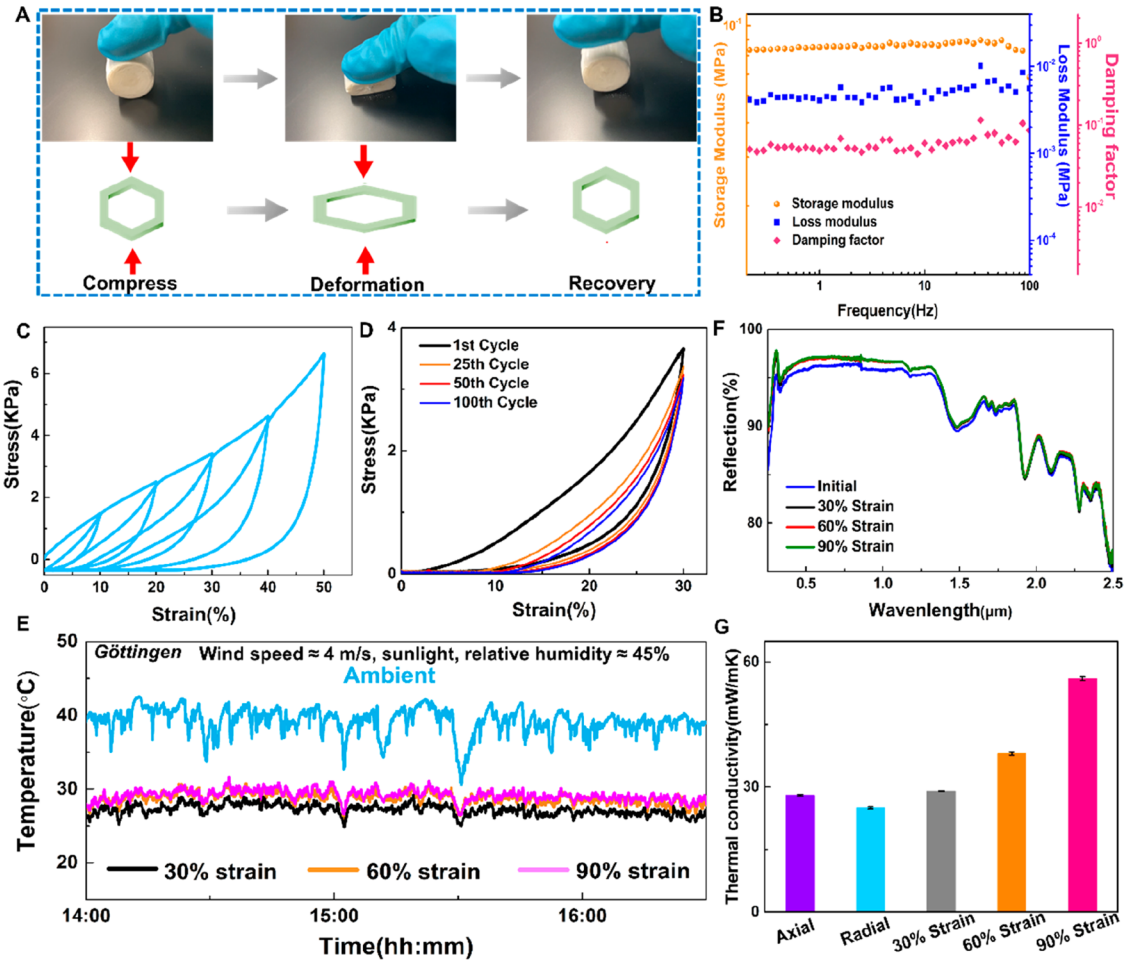

Figure 4. Tunable cooling performance of aerogel cooler. (A) Demonstration and mechanism of compressing-recovering of an aerogel cooler. (B) Frequency dependence of the damping ratio, loss modulus, and storage modulus of aerogel coolers. (C) Compression−release curves of aerogel coolers from 10 to 50% strain. (D) Compression−release curves of aerogel coolers at 30% strain after 100 cycles. (E) Daytime radiative cooling performance of aerogel coolers at different compression ratios. (F) Reflectance of aerogel coolers at different compression ratios. (G) Thermal conductivity of aerogel coolers at different compression ratios.

weather conditions was the synergistic result of a visibly white color of the aerogels (high solar reflectance), infrared (IR) black (high IR emissivity in transparent window), and humidity resistance. As a comparison, aerogels with a random structure without unidirectional channels were also prepared (Figure S14). Such aerogels with a random structure exhibited poor daytime radiative cooling performance and weak mechanical stability (Figure S15). Moreover, we tested cooling performance of aerogel coolers with different thickness to achieve optimized performance (Figure S16). With the thickness increases from 4 to 8 mm, no obvious improvement in cooling performance of aerogel coolers was found. Interestingly, the aerogel cooler with a thickness of 12 mm showed enhanced cooling performance, which should be increased amount of dense nano/micro-structures within the aerogels and at the same time longer thermal conductive pathway.

As shown in Figure 4C and Movie S1, the aerogel coolers can be repeatedly compressed to different strains (from 10 to 50%). Dynamic compression tests showed that the loss modulus and storage were nearly stable and independent of the angular frequency upon 3 orders of magnitude from 0.2 to 100 Hz. In the entire tested angular frequency range, a damping ratio of 0.1−0.2 indicates the dominant elastic property, which should be attributed to the cross-linked CNC networks (Figure 4A,B). Hysteresis curves for 100 compressing-releasing cycles at a strain of 30% showed only slight plastic deformation with ca. 88.4% of the initial stress remaining (Figures 4D and S17). The temperature-invariant elasticity of the aerogel coolers is further explored, as shown in Figures S18 and S19. The damping ratio, loss modulus, and storage modulus showed durable trend from room temperature to nearly 200 °C.

Based on above results, the aerogel coolers exhibited for the first time the mechanically adaptive cooling performance (Figures 4E and S20). At different compression strains (30, 60, and 90%), aerogel cooler showed distinct cooling performance in real applications. The variable cooling ability decreased with increasing strains from 30% to 60% to 90% (Figure 4E). It should be noted that the reflectance and infrared emittance of aerogel coolers at different compression strains did not significantly change (Figures 4F and S21). Therefore, the alteration of cooling performance should be attributed to the change in thermal conductivity because of deformed nano-/microstructures inside the aerogel coolers. Under compression, the air gaps between layers are minimized and the distance between layers decreases, resulting in elevated thermal conductivity from 0.029 W/mK to 0.038 W/mK to 0.056 W/mK, as shown in Figures 4G and S21. This tunable cooling performance based on the enhanced elasticity of the aerogel

https://doi.org/10.1021/acs.nanolett.2c00844
Nano Lett. 2022, 22, 4106−4114

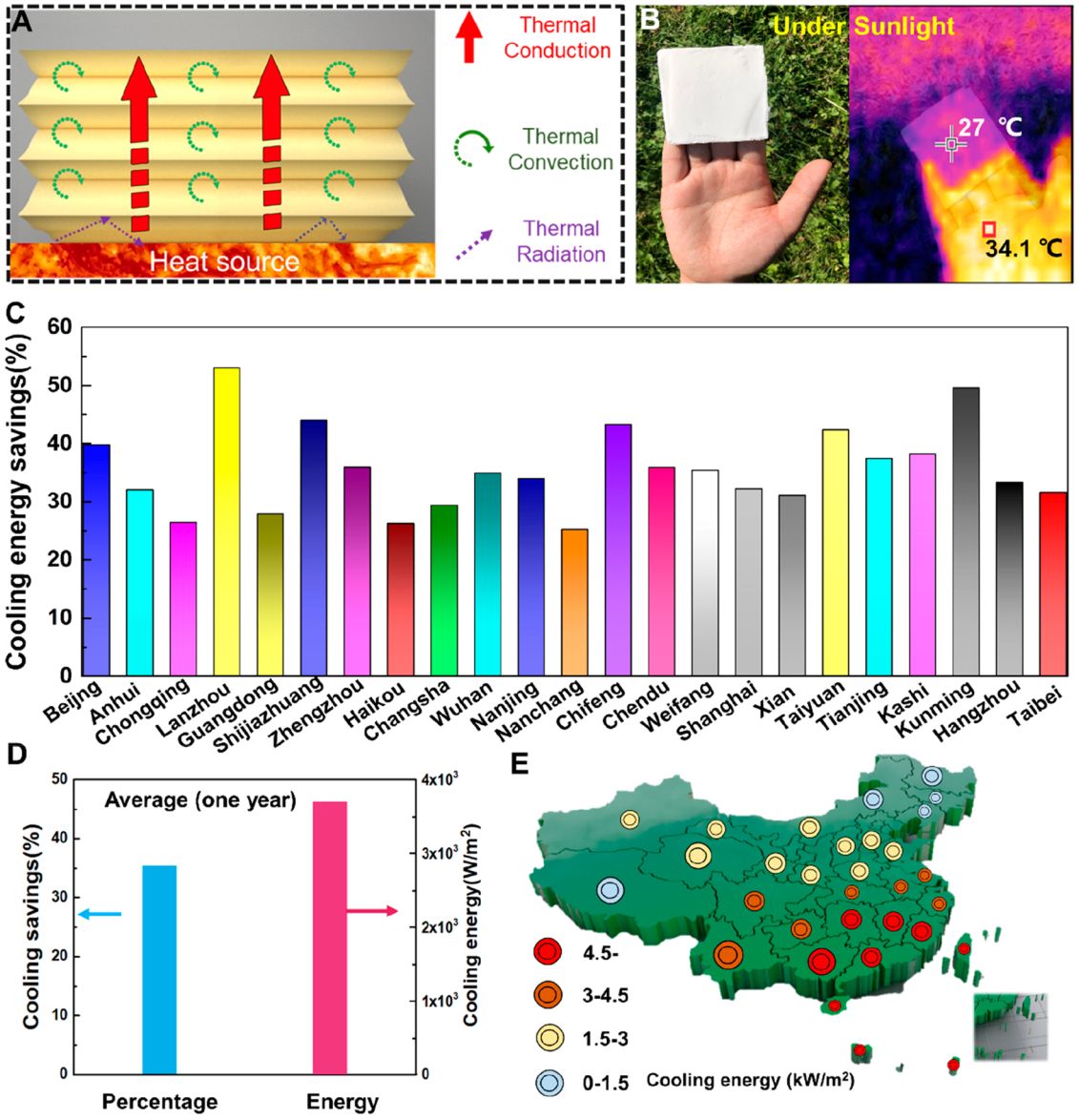

Figure 5. Simulating energy savings of buildings wall and roof by using aerogel coolers. (A) Processes ascribed to thermal insulating property of aerogel coolers. (B) Optical and IR images of human hand covered with an aerogel cooler under sunlight. (C) Total cooling energy savings of 23 cities in China. (D) Total cooling energy saving percentage in China from simulation. (E) Total predicted cooling energy savings of buildings extended for all China cities.

coolers provides a great potential to meet different cooling requirement in various regions all over the world and in distinct weather conditions by simply changing the compression ratios.

Different from traditional radiation coolers, such as nanoporous PE,[15] PVDF fabric,[33] white wood,[14] and cellulose paper[34] displaying poor thermal insulation properties, our aerogel coolers exhibited a intrinsic combination of low thermal conductivity, high IR emittance, and high light reflectance and therefore can offer considerable advantages in thermal regulation. As illustrated in Figure 5A, the excellent thermal insulating character of the aerogel coolers can be explained as follows: (1) Radiation heat transfer is limited because cellulose nanocrystal is an efficient infrared absorber. (2) The hierarchically defined and homogeneous ordered porous nano-/microstructures decreased the heat conduction within solid phase. As shown in Figure S22, the obvious temperature difference between the top and bottom surfaces of the aerogel cooler also confirmed the excellent thermal insulation property. We also visually compared the thermal insulating property of the aerogel cooler with several commercial materials including PS foam, PE, and white paper (Figure S23). After 5 min of heating (80 °C), aerogel cooler exhibited the lowest surface temperature of 41.4 °C.

By detecting the temperature difference between the aerogel cooler and the hand under direct sunlight, the obvious temperature difference showed combined cooling and thermal isolation of the aerogel cooler, as can be observed via an IR camera in Figure 5B. Furthermore, the aerogel coolers can be used to cool the electronics under sunlight (Figure S24). The excellent sunlight reflectance and exceptional daytime radiative cooling ability decreased the surface temperature of laptop surface. As well, the combination of excellent mechanical robustness, cooling performance, and thermal isolation make the aerogel cooler good candidate in protecting freshness of food during hot days (Figure S25). For instance, under sunlight (temperature: 20−25 °C, relative humidity: 40−60%), lemons

https://doi.org/10.1021/acs.nanolett.2c00844
Nano Lett. 2022, 22, 4106−4114

quickly lost water and shriveled the next day (14 h in sunlight). In comparison, no significant water loss or shrinkage was observed for lemons stored in aerogel coolers even after 20 h in sunlight.

Additionally, our aerogel coolers can be easily scaled up and assembled into bulks with different sizes and geometries, which can meet various requirements during applications (Figure S26). The EnergyPlus was used to simulate the influence of different coolers on associated changes in cooling energy demands and building energy balance. The energy-saving modeling process was conducted based on baseline wall and roof material properties and aerogel cooler performance to predict an energy-consumption, as shown in Figure S27. Twenty-three cities in China were selected for this study (thermal zones in China), which can expand results of energy savings to whole country. Our cooling energy savings of the aerogel cooler on outer surfaces of buildings were shown in Figure S28; Haikou (6.89 kW/m^2), Taipei (5.61 kW/m^2), Changsha (4.96 kW/m^2), Wuhan (4.91 kW/m^2), and Nanchang (4.89 kW/m^2) possess the highest cooling energy in the chosen 23 cities in China. Importantly, cities in the southwest region may be suitable for the use of this aerogel cooler to decrease energy consumption of cooling. On the basis of the results, we found that the as prepared aerogel cooler exhibited an obvious energy-saving performance, as shown in Figure 5C. Due to the very dry and hot weather of Lanzhou, it possesses the highest potential cooling savings. Specifically, compared with the traditional building consumption, the aerogel cooler could save 35.4% cooling energy on average (Figure 5D). On the basis of above results, we proposed the energy-saving map in China for a typical year (Figure 5E). Therefore, we can assemble our aerogels into large scale bulks to cover the roofs or the walls with only 1 cm thickness; the highly thermal management of house (efficient radiative cooling and thermal insulation) can be easily realized, resulting in reducing the energy consumption during the whole year in China.

In conclusion, we developed a type of highly cooling and thermal insulating radiative CNC aerogel coolers via a unidirectional freeze casting process. Benefiting from the coexistence of engineered hierarchical structures with integrated nano/microscale structures and chemical bonds at molecular level, such aerogel coolers exhibit superior solar-reflectance (96%), high infrared emittance (92%), and ultralow thermal conduction (0.026 W/mK). It can achieve a subambient temperature drop of up to 9.2 °C under direct sunlight and promisingly ∼7.4 °C even in the hot, moist, and fickle weather conditions with a relative humidity of ∼70%. The cooling performance of the cooling aerogels can be easily dynamically tuned by controlling the compression process. Specifically, the aerogel cooler could save 35.4% cooling energy on average compared to the traditional building consumption. This new strategy of using aerogels provides a novel aspect for developing the tailored and high-performance radiative cooling technology toward reduction in global warming and energy consumption.

■ ASSOCIATED CONTENT

Supporting Information

The Supporting Information is available free of charge at https://pubs.acs.org/doi/10.1021/acs.nanolett.2c00844.

Experimental section; calculation of solar reflectivity and thermal emissivity; calculation of cooling power; simulation of energy savings of aerogel cooler in China; TEM image of CNCs; surface wetting property of pristine CNC aerogel; relative humidity; nighttime cooling performance of CNC aerogel cooler; cooling performance of different surfaces of CNC aerogel coolers; cooling performance of CNC aerogel coolers: conventional freeze casting (random structure) versus directional freeze casting (aligned porous structure); cooling performance of CNC aerogel coolers with different thickness; stress remaining after compressive cycles; dynamic mechanic properties of aerogel cooler; modular assembly process of aerogel coolers; thermal insulating property of aerogel cooler (PDF)

Movie S1: aerogel coolers repeatedly compressed to different strains (MP4)

■ AUTHOR INFORMATION

Corresponding Authors

Yu Fu − *Co-Innovation Center of Efficient Processing and Utilization of Forest Resource, School of Materials Science and Engineering, Nanjing Forestry University, Nanjing, Jiangsu 210037, China;* orcid.org/0000-0002-6349-9932; Email: fuyu@wsu.edu

Kai Zhang − *Sustainable Materials and Chemistry, Department of Wood Technology and Wood-based Composites, Georg-August-University of Göttingen, Göttingen 37077, Germany;* orcid.org/0000-0002-5783-946X; Email: kai.zhang@uni-goettingen.de

Authors

Chenyang Cai − *Co-Innovation Center of Efficient Processing and Utilization of Forest Resource, School of Materials Science and Engineering, Nanjing Forestry University, Nanjing, Jiangsu 210037, China; Sustainable Materials and Chemistry, Department of Wood Technology and Wood-based Composites, Georg-August-University of Göttingen, Göttingen 37077, Germany;* orcid.org/0000-0002-3685-0475

Zechang Wei − *Co-Innovation Center of Efficient Processing and Utilization of Forest Resource, School of Materials Science and Engineering, Nanjing Forestry University, Nanjing, Jiangsu 210037, China*

Chunxiang Ding − *Co-Innovation Center of Efficient Processing and Utilization of Forest Resource, School of Materials Science and Engineering, Nanjing Forestry University, Nanjing, Jiangsu 210037, China;* orcid.org/0000-0002-9344-1010

Bianjing Sun − *Sustainable Materials and Chemistry, Department of Wood Technology and Wood-based Composites, Georg-August-University of Göttingen, Göttingen 37077, Germany*

Wenbo Chen − *Sustainable Materials and Chemistry, Department of Wood Technology and Wood-based Composites, Georg-August-University of Göttingen, Göttingen 37077, Germany*

Christoph Gerhard − *Faculty of Engineering and Health, University of Applied Sciences and Arts, Göttingen 37085, Germany*

Evgeny Nimerovsky − *NMR-based Structural Biology Max-Planck-Institute for Biophysical Chemistry, Göttingen 37077, Germany;* orcid.org/0000-0003-3002-0718

Complete contact information is available at: https://pubs.acs.org/10.1021/acs.nanolett.2c00844

https://doi.org/10.1021/acs.nanolett.2c00844
Nano Lett. 2022, 22, 4106−4114

Author Contributions

[⊥]C.C. and Z.W. contributed equally to this paper.

Notes

The authors declare no competing financial interest.

■ ACKNOWLEDGMENTS

K.Z. thanks the German Research Foundation (DFG) and Lower Saxony Ministry of Science and Culture for the project INST186/1281-1/FUGG. C.C. is grateful for the support of the National Natural Science Foundation of China (Grant No. 31770608), Jiangsu Specially appointed Professorship Program (Sujiaoshi [2016]20), Science and Technology Innovation Project for Overseas Students of Nanjing City (Ningrenshehan [2018]214), the Postgraduate Research & Practice Innovation Program of Jiangsu Province [Grant No. KYCX21_0891], National First-class Disciplines (PNFD), and Jiangsu Government Scholarship for Overseas Studies (JS-2020-195). B.S. and W.C. thank China Scholarship Council for financially supporting their Ph.D. study. We thank Dr. Loren Andreas and Dr. Kai Xue from the Max-Planck-Institute for Biophysical Chemistry for supporting NMR test.

■ REFERENCES

(1) Munday, J. N. Tackling Climate Change through Radiative Cooling. *Joule* **2019**, *3* (9), 2057−2060.
(2) Zhai, Y.; Ma, Y.; David, S. N.; Zhao, D.; Lou, R.; Tan, G.; Yang, R.; Yin, X. Scalable-manufactured randomized glass-polymer hybrid metamaterial for daytime radiative cooling. *Science* **2017**, *355* (6329), 1062−1066.
(3) Li, D.; Liu, X.; Li, W.; Lin, Z.; Zhu, B.; Li, Z.; Li, J.; Li, B.; Fan, S.; Xie, J.; Zhu, J. Scalable and hierarchically designed polymer film as a selective thermal emitter for high-performance all-day radiative cooling. *Nat. Nanotechnol.* **2021**, *16* (2), 153−158.
(4) Zeng, S.; Pian, S.; Su, M.; Wang, Z.; Wu, M.; Liu, X.; Chen, M.; Xiang, Y.; Wu, J.; Zhang, M.; Cen, Q.; Tang, Y.; Zhou, X.; Huang, Z.; Wang, R.; Tunuhe, A.; Sun, X.; Xia, Z.; Tian, M.; Chen, M.; Ma, X.; Yang, L.; Zhou, J.; Zhou, H.; Yang, Q.; Li, X.; Ma, Y.; Tao, G. Hierarchical-morphology metafabric for scalable passive daytime radiative cooling. *Science* **2021**, *373* (6555), 692−696.
(5) Li, X.; Xie, W.; Sui, C.; Hsu, P.-C. Multispectral Thermal Management Designs for Net-Zero Energy Buildings. *ACS Materials Letters* **2020**, *2* (12), 1624−1643.
(6) Zhang, X. A.; Yu, S.; Xu, B.; Li, M.; Peng, Z.; Wang, Y.; Deng, S.; Wu, X.; Wu, Z.; Ouyang, M.; Wang, Y. Dynamic gating of infrared radiation in a textile. *Science* **2019**, *363* (6427), 619−623.
(7) Peng, Y.; Chen, J.; Song, A. Y.; Catrysse, P. B.; Hsu, P.-C.; Cai, L.; Liu, B.; Zhu, Y.; Zhou, G.; Wu, D. S.; Lee, H. R.; Fan, S.; Cui, Y. Nanoporous polyethylene microfibres for large-scale radiative cooling fabric. *Nature Sustainability* **2018**, *1* (2), 105−112.
(8) Wu, J.; He, J.; Yin, K.; Zhu, Z.; Xiao, S.; Wu, Z.; Duan, J.-A. Robust Hierarchical Porous PTFE Film Fabricated via Femtosecond Laser for Self-Cleaning Passive Cooling. *Nano Lett.* **2021**, *21* (10), 4209−4216.
(9) Zhu, L.; Raman, A. P.; Fan, S. Radiative cooling of solar absorbers using a visibly transparent photonic crystal thermal blackbody. *Proc. Natl. Acad. Sci. U. S. A.* **2015**, *112* (40), 12282−12287.
(10) Zhu, R.; Hu, D.; Chen, Z.; Xu, X.; Zou, Y.; Wang, L.; Gu, Y. Plasmon-Enhanced Infrared Emission Approaching the Theoretical Limit of Radiative Cooling Ability. *Nano Lett.* **2020**, *20* (10), 6974−6980.
(11) Mandal, J.; Fu, Y.; Overvig, A. C.; Jia, M.; Sun, K.; Shi, N. N.; Zhou, H.; Xiao, X.; Yu, N.; Yang, Y. Hierarchically porous polymer coatings for highly efficient passive daytime radiative cooling. *Science* **2018**, *362* (6412), 315−319.
(12) Xiang, B.; Zhang, R.; Luo, Y.; Zhang, S.; Xu, L.; Min, H.; Tang, S.; Meng, X. 3D porous polymer film with designed pore architecture and auto-deposited SiO2 for highly efficient passive radiative cooling. *Nano Energy* **2021**, *81*, 105600.
(13) Zhong, H.; Li, Y.; Zhang, P.; Gao, S.; Liu, B.; Wang, Y.; Meng, T.; Zhou, Y.; Hou, H.; Xue, C.; Zhao, Y.; Wang, Z. Hierarchically Hollow Microfibers as a Scalable and Effective Thermal Insulating Cooler for Buildings. *ACS Nano* **2021**, *15* (6), 10076−10083.
(14) Li, T.; Zhai, Y.; He, S.; Gan, W.; Wei, Z.; Heidarinejad, M.; Dalgo, D.; Mi, R.; Zhao, X.; Song, J.; Dai, J.; Chen, C.; Aili, A.; Vellore, A.; Martini, A.; Yang, R.; Srebric, J.; Yin, X.; Hu, L. A radiative cooling structural material. *Science* **2019**, *364* (6442), 760−763.
(15) Zhou, K.; Li, W.; Patel, B. B.; Tao, R.; Chang, Y.; Fan, S.; Diao, Y.; Cai, L. Three-Dimensional Printable Nanoporous Polymer Matrix Composites for Daytime Radiative Cooling. *Nano Lett.* **2021**, *21* (3), 1493−1499.
(16) Zhang, H.; Ly, K. C. S.; Liu, X.; Chen, Z.; Yan, M.; Wu, Z.; Wang, X.; Zheng, Y.; Zhou, H.; Fan, T. Biologically inspired flexible photonic films for efficient passive radiative cooling. *Proc. Natl. Acad. Sci. U. S. A.* **2020**, *117* (26), 14657−14666.
(17) Raman, A. P.; Anoma, M. A.; Zhu, L.; Rephaeli, E.; Fan, S. Passive radiative cooling below ambient air temperature under direct sunlight. *Nature* **2014**, *515* (7528), 540−544.
(18) Wang, T.; Wu, Y.; Shi, L.; Hu, X.; Chen, M.; Wu, L. A structural polymer for highly efficient all-day passive radiative cooling. *Nat. Commun.* **2021**, *12* (1), 365.
(19) Gamage, S.; Banerjee, D.; Alam, M. M.; Hallberg, T.; Åkerlind, C.; Sultana, A.; Shanker, R.; Berggren, M.; Crispin, X.; Kariis, H.; Zhao, D.; Jonsson, M. P. Reflective and transparent cellulose-based passive radiative coolers. *Cellulose* **2021**, *28* (14), 9383−9393.
(20) Gamage, S.; Kang, E. S. H.; Åkerlind, C.; Sardar, S.; Edberg, J.; Kariis, H.; Ederth, T.; Berggren, M.; Jonsson, M. P. Transparent nanocellulose metamaterial enables controlled optical diffusion and radiative cooling. *Journal of Materials Chemistry C* **2020**, *8* (34), 11687−11694.
(21) Cai, C.; Wei, Z.; Huang, Y.; Wang, P.; Song, J.; Deng, L.; Fu, Y. Bioinspired structure-robust cellulose nanocrystal films with enhanced water resistance, photothermal conversion ability, and fluorescence. *Cellulose* **2020**, *27* (17), 10241−10257.
(22) Cheng, Q.; Huang, C.; Tomsia, A. P. Freeze Casting for Assembling Bioinspired Structural Materials. *Adv. Mater.* **2017**, *29* (45), 1703155.
(23) Yu, Z.-L.; Yang, N.; Zhou, L.-C.; Ma, Z.-Y.; Zhu, Y.-B.; Lu, Y.-Y.; Qin, B.; Xing, W.-Y.; Ma, T.; Li, S.-C.; et al. Bioinspired polymeric woods. *Science Advances* **2018**, *4* (8), No. eaat7223.
(24) Zhang, J.; Cheng, Y.; Xu, C.; Gao, M.; Zhu, M.; Jiang, L. Hierarchical Interface Engineering for Advanced Nanocellulosic Hybrid Aerogels with High Compressibility and Multifunctionality. *Adv. Funct. Mater.* **2021**, *31* (19), 2009349.
(25) Cai, C.; Wei, Z.; Huang, Y.; Ding, C.; Wang, P.; Song, J.; Deng, L.; Fu, Y.; Zhong, W. H. Ultralight Programmable Bioinspired Aerogels with an Integrated Multifunctional Surface for Self-Cleaning, Oil Absorption, and Thermal Insulation via Coassembly. *ACS Appl. Mater. Interfaces* **2020**, *12* (9), 11273−11286.
(26) Chen, Y.; Dang, B.; Fu, J.; Wang, C.; Li, C.; Sun, Q.; Li, H. Cellulose-Based Hybrid Structural Material for Radiative Cooling. *Nano Lett.* **2021**, *21* (1), 397−404.
(27) Chen, M.; Pang, D.; Mandal, J.; Chen, X.; Yan, H.; He, Y.; Yu, N.; Yang, Y. Designing Mesoporous Photonic Structures for High-Performance Passive Daytime Radiative Cooling. *Nano Lett.* **2021**, *21* (3), 1412−1418.
(28) Xue, X.; Qiu, M.; Li, Y.; Zhang, Q. M.; Li, S.; Yang, Z.; Feng, C.; Zhang, W.; Dai, J.-G.; Lei, D.; Jin, W.; Xu, L.; Zhang, T.; Qin, J.; Wang, H.; Fan, S. Creating an Eco-Friendly Building Coating with Smart Subambient Radiative Cooling. *Adv. Mater.* **2020**, *32* (42), 1906751.
(29) Leroy, A.; Bhatia, B.; Kelsall, C. C.; Castillejo-Cuberos, A.; Di Capua H., M.; Zhao, L.; Zhang, L.; Guzman, A. M.; Wang, E. N. High-performance subambient radiative cooling enabled by optically selective and thermally insulating polyethylene aerogel. *Science Advances* **2019**, *5* (10), eaat9480.

https://doi.org/10.1021/acs.nanolett.2c00844
Nano Lett. 2022, 22, 4106−4114

(30) Granqvist, C. G.; Hjortsberg, A. Radiative cooling to low temperatures: General considerations and application to selectively emitting SiO films. *J. Appl. Phys.* **1981**, *52* (6), 4205−4220.
(31) Hossain, M. M.; Gu, M. Radiative Cooling: Principles, Progress, and Potentials. *Advanced Science* **2016**, *3* (7), 1500360.
(32) Jaramillo-Fernandez, J.; Yang, H.; Schertel, L.; Whitworth, G. L.; Garcia, P. D.; Vignolini, S.; Sotomayor-Torres, C. M. Highly-Scattering Cellulose-Based Films for Radiative Cooling. *Advanced Science* **2022**, *9* (8), 2104758.
(33) Wang, X.; Liu, X.; Li, Z.; Zhang, H.; Yang, Z.; Zhou, H.; Fan, T. Scalable Flexible Hybrid Membranes with Photonic Structures for Daytime Radiative Cooling. *Adv. Funct. Mater.* **2020**, *30* (5), 1907562.
(34) Tian, Y.; Shao, H.; Liu, X.; Chen, F.; Li, Y.; Tang, C.; Zheng, Y. Superhydrophobic and Recyclable Cellulose-Fiber-Based Composites for High-Efficiency Passive Radiative Cooling. *ACS Appl. Mater. Interfaces* **2021**, *13* (19), 22521−22530.

https://doi.org/10.1021/acs.nanolett.2c00844
Nano Lett. 2022, 22, 4106−4114